

# We are IntechOpen, the world's leading publisher of Open Access books Built by scientists, for scientists

6,900

Open access books available

186,000

International authors and editors

200M

Downloads

Our authors are among the

154

Countries delivered to

TOP 1%

most cited scientists

12.2%

Contributors from top 500 universities



WEB OF SCIENCE™

Selection of our books indexed in the Book Citation Index  
in Web of Science™ Core Collection (BKCI)

Interested in publishing with us?  
Contact [book.department@intechopen.com](mailto:book.department@intechopen.com)

Numbers displayed above are based on latest data collected.  
For more information visit [www.intechopen.com](http://www.intechopen.com)



# Detection and Monitoring of Marine Pollution Using Remote Sensing Technologies

*Sidrah Hafeez, Man Sing Wong, Sawaid Abbas,  
Coco Y.T. Kwok, Janet Nichol, Kwon Ho Lee, Danling Tang  
and Lilian Pun*

## Abstract

Recently, the marine habitat has been under pollution threat, which impacts many human activities as well as human life. Increasing concerns about pollution levels in the oceans and coastal regions have led to multiple approaches for measuring and mitigating marine pollution, in order to achieve sustainable marine water quality. Satellite remote sensing, covering large and remote areas, is considered useful for detecting and monitoring marine pollution. Recent developments in sensor technologies have transformed remote sensing into an effective means of monitoring marine areas. Different remote sensing platforms and sensors have their own capabilities for mapping and monitoring water pollution of different types, characteristics, and concentrations. This chapter will discuss and elaborate the merits and limitations of these remote sensing techniques for mapping oil pollutants, suspended solid concentrations, algal blooms, and floating plastic waste in marine waters.

**Keywords:** remote sensing, water pollution detection and monitoring, optical sensors, oil spill, algal blooms, chlorophyll-a, suspended sediment concentration, marine plastic litter

## 1. Introduction

The oceans act as a natural sink for carbon dioxide and other greenhouse gases. However, anthropogenic activities have severely polluted the marine environment in the past few decades. Pollutants including plastic, oil, toxic chemicals, radioactive waste, and domestic and industrial sewage can be found in marine waters. Marine pollution is also caused by the discharge of sewage into rivers and excessive nutrients entering marine waters from agricultural fertilizers and pesticides [1]. These pollutants have adverse impacts on marine ecosystem including but not limited to sensitive coral reefs, mangroves, and aquaculture [2]. Therefore, in addition to reducing pollutant flow into oceans, it is essential to map and monitor marine pollutants to ensure a sustainable marine ecosystem.

Scientists and researchers have been working on detailed ocean monitoring for a sustainable blue economy. A variety of sensing systems are now available

for ocean monitoring including autonomous underwater vehicles (AUVs), profiling floats, gliders, drifters, volunteer measurements from ships, and sensing nodes with cable networks [3]. These approaches to marine monitoring usually measure temperature, conductivity, pH, salinity, dissolved oxygen, fluorescence due to chlorophyll, turbidity, and color dissolved organic matter (CDOM). The most common approach for marine pollution measurements is to use conventional method of collecting in situ water samples using boats/ships from different depths of water with water samplers. The water samples are analyzed in the laboratory to determine the physical and chemical properties of the water. Such methods are accurate but time-consuming and geographically constrained and require trained professionals and laboratory analysis. However, real-time or near real-time measurements of marine pollutants and toxins across a range of spatial scales are necessary for monitoring and managing the environmental impacts and understanding the processes governing their spatial distribution [3].

To overcome these problems, remote sensing technology provides spatially synoptic and near real-time measurements that can be effectively used to detect, map, and track many pollutants such as oil and chemical spills, algal blooms, and high suspended solid concentrations. Aerial and satellite remote sensing has been demonstrated as an effective tool in detecting and mapping pollutant spills and for providing useful input data for oil spill models, to track pollutants through space and time [4–6]. An added advantage of remote sensing is that it provides information from remote areas. However, existing remote sensing technology still has some limitations, such as estimating pollutants over the vertical dimension of the water column.

The initial premise of watercolor remote sensing was to determine optical water quality variables such as chlorophyll-a (Chl-a) concentration, diffuse attenuation coefficient, and water-leaving radiance spectra [7]. The optical properties of water depend on many factors, e.g., suspended organic and inorganic particles and dissolved substances. There have been many successful applications of using remote sensing sensors for water color monitoring. The coastal zone color scanner (CZCS), having a spatial resolution of 825 m for six spectral bands from 443 to 750 nm, was the earliest satellite sensor designed and launched in 1978 specially to study ocean color. The sea-viewing wide field-of-view sensor (SeaWiFS) was the successor to CZCS with a spatial resolution of 1.1 km for eight spectral bands from 402 to 885 nm. Currently, many satellite sensors provide ocean color data for marine monitoring such as the moderate resolution imaging spectroradiometer (MODIS), the geostationary ocean color imager (GOCI), the visible infrared imager radiometer suite (VIIRS), the ocean and land color imager (OLCI), the Landsat operational land imager (OLI), and the Sentinel-2 multispectral instrument (MSI), all of which have suitable spectral and spatial resolutions capable of detecting marine pollutants and other water quality parameters (**Table 2**).

In order to track marine pollutants, prior understanding of marine dynamics is important, such as ocean current direction and magnitude, direction and speed of surface winds, sea surface temperature (SST), and sea surface salinity (SSS). Remote sensing now provides multiple satellite and airborne sensors to acquire information about marine dynamics over the vast marine regions. Apart from optical data, scanning radiometers and microwave sounders measure SST data, altimeters collect wave height data, and synthetic aperture radar (SAR) can measure the sea surface roughness patterns from which information on sea surface winds can be derived [31]. These datasets are of critical importance for detection and tracking of pollutants.

## 2. Remote sensing of water monitoring

Remote sensors capture the response of the electromagnetic interaction with water (**Figure 1**). Absorption and scattering are inherent optical properties (IOP) of water; and variations in IOP change the reflectance of water which is captured by a remote sensing sensor, and this is known as the apparent optical properties (AOP) of water (**Figure 2**). Reflection, absorption, and transmittance of electromagnetic radiation are highly dependent on the concentrations, types, and presence of substances in water. Total absorption is the sum of absorption by phytoplankton (microalgae), non-algal pigments (NAP), color dissolved organic matter (CDOM), and absorption by water, whereas light scattering by water is mainly controlled by suspended sediments (SS) present in water. Hence, ocean color represents the responses in , green, and red region, and data can be used to estimate the concentrations of water constituents [7].

Generally, clear water has low reflectance in the visible spectrum and has no reflection in near infrared (NIR) region, as it is absorbed by clear water. However, high reflectance measurements in red (600–700 nm) and NIR region (750–1400 nm) show a strong correlation with SS concentrations. A high concentration of suspended sediments blocks the transmittance to and from lower depths and therefore increases reflectance from the water surface. Similarly, high concentrations of chlorophyll (a photosynthetic pigment in phytoplankton and macroalgae) in water cause high reflectance in the green region (500–600 nm) and high absorption in the blue and red regions due to photosynthetic activity (**Figure 2**).

A portion of absorbed incident energy by the earth's features is also re-emitted in the thermal infrared region of the electromagnetic spectrum. Many satellite sensors such as MODIS, VIIRS, the advanced very high-resolution radiometer (AVHRR), and the sea and land surface temperature radiometer (SLSTR) measure the emitted thermal energy to determine sea surface temperature (SST). SST is an important parameter for understanding ocean water circulation. In case of large oil spills, these data can be effective for pinpointing the oil spilled areas, as they appear cooler than water surface due to their lower emissivity [31].

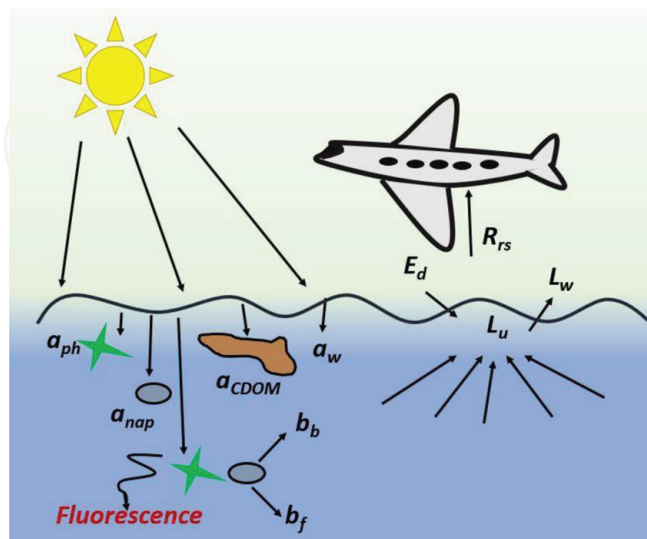


**Figure 1.**

Interaction of light with the water surface.  $a$  is absorption ( $a_{ph}$ , absorption by phytoplankton;  $a_{nap}$ , absorption by non-algal pigments;  $a_{CDOM}$ , absorption by color dissolved organic matter; and  $a_w$ , absorption by water),  $b$  is backscattering ( $b_b$ , backward scattering;  $b_f$ , forward scattering),  $R_{rs}$  is remote sensing reflectance recorded by sensor,  $E_d$  is downwelling irradiance,  $L_u$  is upwelling radiance, and  $L_w$  is water-leaving radiance [32].

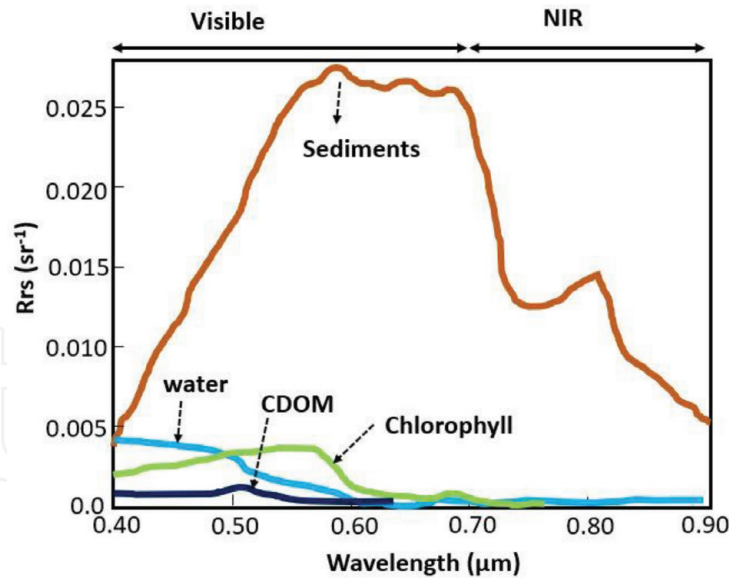


**Figure 2.** Reflectance ( $R_{rs}$ ) by clear water (blue), water with chlorophyll content (green), water with CDOM (black), and sedimented water (orange) [32].

Fluorescence is another type of energy emitted by a substance when it comes to a lower energy level from a higher energy level. The emitted energy is in a longer wavelength than the excitation wavelength. Algae absorb visible light for the photosynthesis process and emit excessive energy in the form of fluorescence signal (681 nm, the fluorescence band) when chlorophyll molecule comes to the non-excitation state during the photosynthesis process. The fluorescence can be detected by optical sensors with fine spectral resolution in the far-red and NIR and has a potential source for monitoring changes in the photosynthesis process in plants. Furthermore, in laser fluorometry, laser light is used to excite molecules [33]. This technique is common to detect oil and chemical spills [31].

## 2.1 Remote sensing platforms and sensors for water monitoring

There are now several remote sensing platforms for monitoring water pollutants, and they can be categorized into two types: airborne and spaceborne.

### 2.1.1 Airborne sensors

An aircraft flies at relatively low altitudes (a few hundred meters to a few kilometers above the surface); therefore, the acquired data always have higher levels of detail. Airborne data are particularly useful for real-time monitoring of oil and chemical spills. Four common airborne sensors used for spill surveillance [34] are listed below:

- i. Infrared/ultraviolet line scan (IR/UVLS)
- ii. Side-looking airborne radar (SLAR)
- iii. Microwave radiometer (MWR)
- iv. Laser fluorosensor (LF)

Airborne hyperspectral sensors with fine spatial resolution are able to capture detailed spectral variations. Therefore, they help to select the appropriate spectral region to study a specific water quality parameter, design satellite sensors, and improve already developed algorithms. Some airborne hyperspectral sensors particularly useful for studying coastal/river water quality are described in **Table 1**.

### 2.1.2 Spaceborne sensors

Spaceborne sensors can cover extensive and remote areas for water quality monitoring. Optical spaceborne sensors used for marine monitoring are mostly in sun-synchronous orbit; only GOCI, designed specifically for marine monitoring, is placed in geostationary orbit. The spatial coverage of these sensors ranges from tens to hundreds of kilometers, and the temporal frequency is from hourly to weekly monitoring.

Many algorithms have been developed to retrieve water quality information such as primary productivity, Chl-a variability, SS, total suspended solids (TSS), turbidity, total nitrogen, total phosphorus, CDOM, and SST. **Table 2** shows the satellite sensors most used for the study of water quality parameters related to marine pollution. The major application areas of active spaceborne sensors include, but are not limited to, sea surface currents, oil spills, biogenic films (algal blooms), and river plumes (**Table 5**).

| Sensor  | Manufacturer               | Number of bands | Spectral range (nm)                    | Spatial resolution (m) | Studied parameter   |
|---|----------------------------|-----------------|--|------------------------|---|
| Airborne visible infrared imaging spectrometer (AVIRIS) | NASA Jet Propulsion Lab    | 224             | 400–2500                               | 17                     | Bottom albedo, water absorption, backscattering coefficients [35], Chl-a, CDOM, TSS [36]      |
| HyMap   | Earth Search Sciences Inc. | 128             | 400–2500                               | 3–10                   | Heavy metals [37]   |
| Portable remote imaging spectrometer (PRISM)            | NASA Jet Propulsion Lab    | —               | 350–1050, SWIR band (1240 and 1640)    | 0.3                    | Sediment, CDOM, chlorophyll fluorescence [38] turbidity, Chl-a, dissolved organic carbon [39] |
| Airborne prism experiment (APEX)                        | VITO (Belgium)             | 313             | VIS and NIR (380–970), SWIR (970–2500) | 2–5                    | Chlorophyll fluorescence, SS [40]   |

**Table 1.**  
*Hyperspectral airborne sensors used in water quality assessment.*

| Satellite sensor  | Launch date       | Spectral bands (nm)   | Spatial resolution (m) | Swath width (km) | Marine parameter accessed                       |
|---|-------------------|---|------------------------|------------------|---|
| <i>Satellite sensors with moderate spatial resolution</i> |                   |   |                        |                  |   |
| Landsats 4 and 5 TM                                       | 1 March 1984      | 5 (450–1750), 1 (2080–2350), and 1 (1040–1250)  | 30–120                 | 185              | Chl-a, SS, Secchi depth [8]                     |
| Landsat 7 ETM+  | 15 April 1999     | 6 (450–1750), 1 Pan (520–900), 1 (2090–2350), and 1 (1040–1250)   | 15–30–60               | 183              | Chl-a, SS, Secchi depth, turbidity [9]          |
| Terra Aster   | 18 December 1999  | 3 (520–860), 6 (1600–2430), and 5 TIR (8125–11,650)   | 15–30–90               | 60               | Chl-a [10]                                      |
| EO-1 ALI  | November 2000     | (443–2350)  | 30                     |                  | Turbidity [11], SS [12]                         |
| EO-1 Hyperion   | 1 November 2000   | 242 (350–2570)  | 30                     | 7.5              | Chl-a, SS, CDOM [13, 14]                        |
| PROBA CHRIS   | 22 October 2001   | 19 (400–105)  | 18–36                  | 14               | Chl-a, phycocyanin [15] behenic macroalgae [16] |
| HICO  | 10 September 2009 | 128 (350–1080)  | 100                    | 45–50            | Chl-a, turbidity, CDOM [17], SS [18]            |
| Landsat 8 OLI/TIRS  | 11 February 2013  | 1 cirrus cloud detection (1360–1380), 5 (430–880), 1 Pan (500–680), 2 (1570–2290), 2 TIRS (10,600–12,510) | 15–30–100              | 170              | Chl-a, SS, turbidity, TN, TP [19]               |
| Sentinel-2 MSI  | 23 June 2015      | 8 (490–865), 1(443) coastal aerosol, and 3 (1375–2190)  | 10–20–60               | 290              | Chl-a, CDOM, DOC [20], SS [21]                  |
| <i>Satellite sensors for regional coverage</i>            |                   |   |                        |                  |   |
| Orb View 2 SeaWiFS  | 1 August 1997     | 8 (402–885)   | 1130                   | 2806             | Chl-a [22]                                      |
| Terra, Aqua MODIS   | 18 December 1999  | 2 (620–876), 5 (459–2155), 29 (405–877), and thermal  | 250–500–100            | 2330             | Chl-a, CDOM SS [23], turbidity [24], TP [25]    |
| ENVISAT-1 MERIS   | 1 March 2002      | 15 (390–1040)   | 300–1200               | 1150             | Chl-a, SS [26, 27]                              |
| GOCI  | 26 June 2010      | 8 (412–865)   | 500                    | 2500             | Chl-a, SS, turbidity [28]                       |
| Suomi NPP VIIRS   | 28 October 2011   | 5 bands (640–1145), 16 bands (412–12,013), DNB (500–900)  | 375–750                | 3060             | Chl-a [29]                                      |
| Sentinel-3 OLCI   | 16 February 2016  | 21 (400–1020)   | 300                    | 1270             | Chl-a, SS, CDOM, and Secchi depth [30]          |

**Table 2.**  
Satellite sensors mostly used to retrieve marine water quality parameters.

### 3. Remote sensing for marine monitoring

#### 3.1 Chlorophyll (Chl-a) and algal blooms

Most algal species are nontoxic and are always present in coastal and open oceans. Planktons are the base of the marine food chain [22]. But, algae do not have to produce toxins to be harmful to the environment. The accelerated growth of algae produces a large amount of biomass which blocks sunlight and produces an anoxic or hypoxic condition (dissolved oxygen is depleted from the water column), which is hazardous to marine life. Algal blooms also affect coastal operations such as movement of ships, coastal tourism, and coastal sports (**Figure 3**). Algal blooms can persist from a few days to more than a month and spatially they may extend from a few meters to tens of kilometers.

The impact of algal blooms on marine life depends largely on the algal species involved. In situ field data collected using vessels are important for determining the algal species and level of toxicity during the bloom. However, field data are always limited for estimating the spatial extent as well as the dispersion. Detection of algal bloom by estimating the Chl-a concentrations using satellite imagery has been well-researched, as remote sensing has been used to observe ocean primary productivity since the launch of CZCS in 1978. High spatial and temporal resolutions are the main requirements of remote sensing data to study the variability in ocean and coastal Chl-a. By comparing a time series of satellite images, researchers can evaluate the spatial and temporal variations in Chl-a concentration during the bloom. This can also help to understand the dynamics of blooms. However, there are still certain conditions for using optical remote sensing to detect Chl-a, including (i) no or low cloud cover, (ii) the bloom should be near to the surface, and (iii) the bloom must cause the coloration of the water.

Optical remote sensing can observe the coloration of water due to algal pigments. In the open ocean, the color of water is mainly determined by phytoplankton; hence, it is relatively simple to develop algorithms using a bio-optical approach and remote sensing reflectance [22]. In the open ocean, Chl-a can be retrieved from the ratio of blue and green wavelengths as Chl-a absorption is sensitive to blue wavelength and reflectance peak occurs in the green wavelength region [22]. However, in coastal waters, the color of water also depends on organic matter such as NAP, CDOM, and inorganic solids, and consequently it is more complex to determine accurate Chl-a concentrations in coastal/turbid waters. Researchers have demonstrated that waters with increased Chl-a concentrations show a lower



**Figure 3.** Spread of green algae along the coast of Qingdao in 2008, when summer Olympics was planned in this coast (source: Corey Sheran/Flickr) (right) and algae visible in MODIS false color image (shortwave, NIR, and Red) (source: MODIS rapid response project at NASA/GSFC) (left).

spectral response at short wavelengths especially in the blue wavelength regions [41]. This is due to increased absorption of red and blue wavelengths during photosynthetic process. **Figure 4** shows the reflectance of water with increasing Chl-a concentrations. Thus, in coastal waters, the red/NIR ratio is more effective for retrieval of Chl-a due to the presence of suspended solids and the increased spectral response of Chl-a pigments at longer wavelengths [43].

Narrow spectral bandwidth is a necessity for accurate retrieval of Chl-a concentrations [7]. The height of the spectral peak between 700 and 710 nm is used as a proxy for phytoplankton biomass [44]. Many researchers have used broad wavelength data (i.e., Landsat, HJ-1A/1B) as input to regression and neural network approaches for estimating Chl-a, achieving reasonable accuracy (70–90%) [9, 19, 45, 46].

**Table 3** shows some studies and datasets used to study Chl-a in marine regions. Lim and Choi [19] found that green and NIR bands of OLI are highly correlated with Chl-a ( $R = 0.71$ ) in Korean waters. Nazeer and Nichol [46] also used the red/blue ratio to retrieve Chl-a with high accuracy ( $R = 0.85$ ). Gurlin et al. [43] calibrated three models for Chl-a concentrations from 0 to  $100 \text{ mg m}^{-3}$  using two bands (red and NIR) of MERIS and MODIS reflectance data. They found that a simple two-band model achieved a higher accuracy than a complex three-band model. Moses et al. [51] also calibrated a red-NIR algorithm for high Chl-a concentrations in productive turbid waters. **Figure 5** shows Chl-a concentrations in highly turbid Pearl River Estuary and connecting rivers, derived using high-resolution MSI data with the method of Moses et al. [51].

Recently, machine learning approaches taking advantages of reflectance in all bands have also been applied using Landsat [45, 52] and GOCI data [28]. Our work also shows the potential use of Landsat TM, ETM+, and OLI with a machine learning approach to estimate Chl-a in coastal waters (**Figure 6**). We have evaluated three machine learning models to estimate Chl-a in the coastal waters of Hong Kong, of which artificial neural networks (ANN) performed best resulting in higher  $R$  (0.91) and lower RMSE ( $1.4 \text{ } \mu\text{g/L}$ ) than models based on support vector regression (SVR) and random forest (RF) algorithms. Chlorophyll indices such as the cyanobacteria index [53], maximum chlorophyll Index [54], and maximum peak height algorithm [55] have been demonstrated the robustness for detecting algal blooms and surface scum in coastal waters. Lunetta et al. [56] described the potential of using cyanobacteria index to measure cyanobacteria cell counts in bloom situations using MERIS data. Nazeer et al. [57] used board waveband band data (Landsat TM, ETM+, and HJ-1A/1B CCD) along with meteorological data as inputs to an artificial neural network model to map phytoplankton cell counts

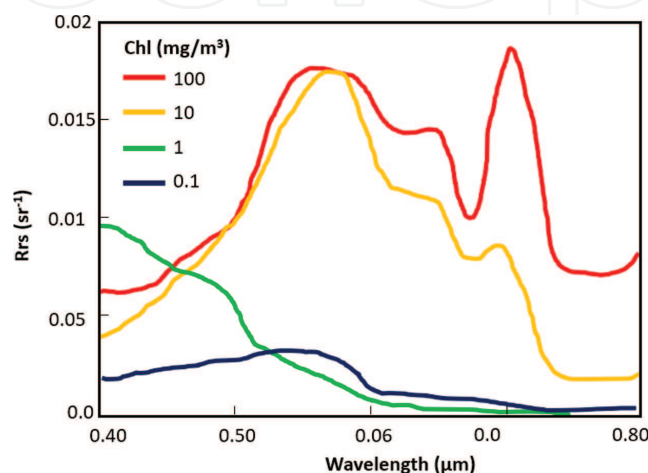


**Figure 4.** Changing spectral response of water with different levels of chlorophyll concentration [42].

| Band combination   | Sensor                             | Reference                            |      |
|--|------------------------------------|--------------------------------------|------|
| All bands (neural network and other machine learning methods)          | GOCI                               | [28]                                 |      |
|  | TM, SAR                            | [45]                                 |      |
| Multiple bands and their ratios (multiple regression)                  | OLI band (2–5)                     | [19]                                 |      |
|  | OLCI                               | [30]                                 |      |
|  | TM                                 | [8]                                  |      |
|  | HICO                               | [17]                                 |      |
| Blue (400–500 nm) and green (500–600 nm) ratio                         | In situ                            | [22]                                 |      |
| Blue (400–500 nm) and red (600–700 nm) ratio                           | TM, ETM+, HJ-1A/1B<br>CCD          | [9, 46]                              |      |
| Green (500–600 nm) and red (600–700 nm) ratio                          | TM                                 | [47]                                 |      |
|  | In situ (0.70/0.56 $\mu\text{m}$ ) | [44]                                 |      |
| Red (600–700 nm) and NIR (700 $\mu\text{m}$ –900 $\mu\text{m}$ ) ratio | MERIS, MODIS                       | [43]                                 |      |
|  | HICO                               | [48]                                 |      |
| Using a single band  | Green (500–600 nm)                 | Daedalus Airborne<br>Thematic Mapper | [49] |
|  | Red (600–700 nm)                   | AVHRR                                | [50] |

**Table 3.**  
 Methods used to retrieve Chl-a using remote sensing data in the river and marine waters.

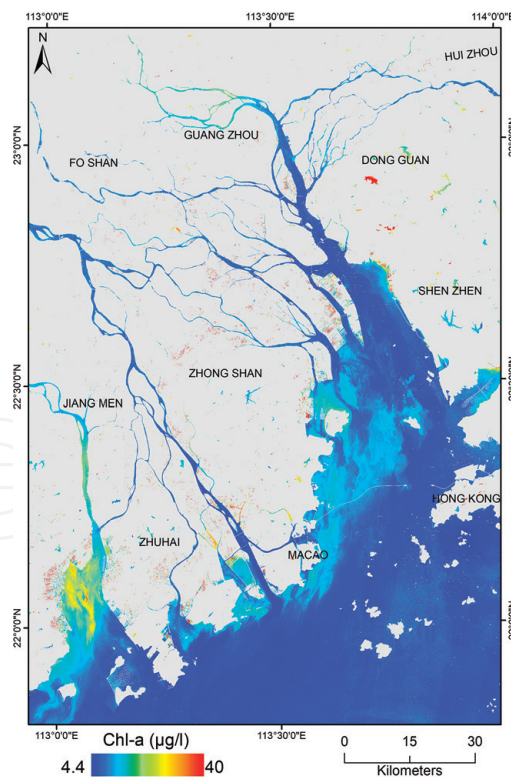


**Figure 5.**  
 Chl-a concentration observed in the Pearl River Estuary and its connecting rivers on 31 December 2017.

during a bloom in the complex coastal waters of Hong Kong and validated the model in two lakes in the United States and Japan.

Synthetic aperture radar (SAR) data can also be used to detect large algal blooms in cloudy weather as algal blooms may appear as an area of low backscatter compared to surrounding water surfaces [50].

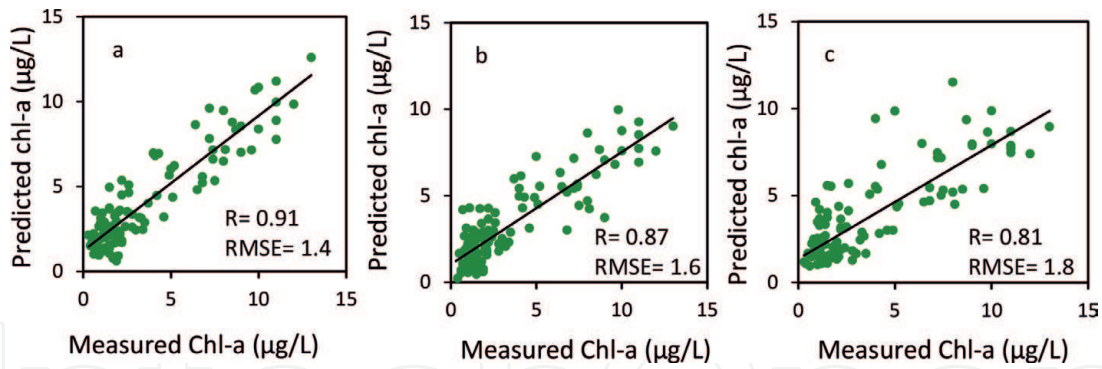


**Figure 6.** Comparison of measured and predicted values from three machine learning models. (a) Chl-a concentration using artificial neural network, (b) Chl-a concentration using support vector regression, and (c) Chl-a concentration using random forest.

### 3.2 Turbidity, total suspended sediments, and stormwater runoff plumes

Turbidity is an optical property of water and is highly influenced by concentrations of suspended and dissolved organic and inorganic materials in water, including Chl-a, SS, and CDOM. SS is mainly responsible for the light scattering, whereas CDOM and Chl-a control the light absorption properties of water [58].

Turbidity and TSS are two important variables of marine systems studies because of their direct linkages with photosynthetically available radiation, which affects the growth of plankton and other algae [41]. Turbidity has also been used to measure fluvial SS concentrations in rivers and river plumes [59]. These fluvial SS loads are rich in nutrients and considered a cause of eutrophication. So, it is vital to have time series records of suspended sediment concentrations for better understanding of land-ocean interactions. High SS loads negatively affect aquaculture [59] and are hazardous to benthic invertebrates [60]. These parameters are also associated with the diffuse attenuation coefficient (penetration of light, in the blue-green region of the spectrum, through water column) and Secchi disk depth (a measure of water transparency) [41]. For all these reasons, turbidity and TSS concentrations are considered to be critical parameters in the study of marine systems.

Ocean color remote sensing techniques are widely used to monitor spatiotemporal variations in SS concentration and for mapping of water turbidity. **Figure 7** shows the changes in ocean color due to high sediment loads in the Yangtze River Estuary [60] and the Pearl River Estuary [61]. It is suggested that an algorithm using single bands provides a good estimation of TSS concentrations if an appropriate band is used [62]. Moreover Novo et al. [63] and Curran et al. [64] have demonstrated that a single-band approach may be adopted when water reflectance in the single band has a linear relationship with TSS concentrations. However, coastal water often consists of a complex mixture of substances and results in large variations in reflectance. In this case, multiple spectral bands should be adopted for TSS retrieval [62, 65, 66]. These methods using band arithmetic can achieve high accuracy around 80% for retrieving TSS concentrations in complex waters [67, 68]. The peak of the reflectance curve shifts from the green region to the red region with increasing concentration of dissolved and suspended matter; and water starts reflecting significantly in NIR region [21] (**Figure 8**). For water with high TSS concentrations, the spectral region between 600 and 900 nm should be used. Several studies using Landsat TM, ETM+, and OLI show that the blue, green, red, and NIR bands are useful for the determination of TSS [8, 19, 68–70]. Literature also shows that TM, ETM+, OLI, and MODIS are the most frequently used sensors for developing algorithms to study seasonal TSS variability in coastal and estuarine



**Figure 7.** Terra-MODIS true color image, captured on 16 September 2000, shows the sediment plume of the Yangtze River Estuary (left). The Sentinel-2 true color image, captured on 31 December 2017, shows high sediment concentrations in the Pearl River Estuary (right).

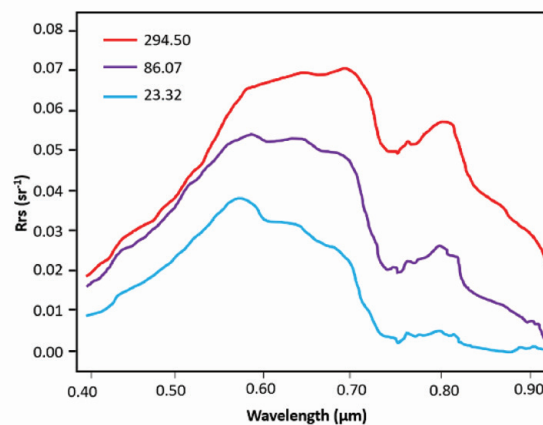


**Figure 8.** Remote sensing reflectance ( $R_{rs}$ ) spectra of water containing different suspended solid concentration (mg/L) [21].

areas, due to the large amount of archived remote sensing data [24, 71, 72]. The recently launched MSI sensor onboard Sentinel-2A and Sentinel-2B provide high spatial resolution of 10–20 m with a high temporal resolution of 5 days. The high spatial resolution (10 m) red and NIR bands are capable of routine monitoring of TSS concentration and turbidity in narrow bays, rivers, and inlets. **Figure 9** shows the suspended matter concentrations, and **Figure 10** shows turbidity in the Pearl River Estuary and connecting rivers using MSI data with algorithms of Nechad et al. [62] and Nechad et al. [73], respectively.

Methods and algorithms for estimation of TSS and turbidity have been evolved from simple methods such as linear/nonlinear regression and principal component analysis (PCA) to relatively complex techniques such as genetic algorithms and ANN. Nazeer and Nichol [68] initially developed a regression model resulting

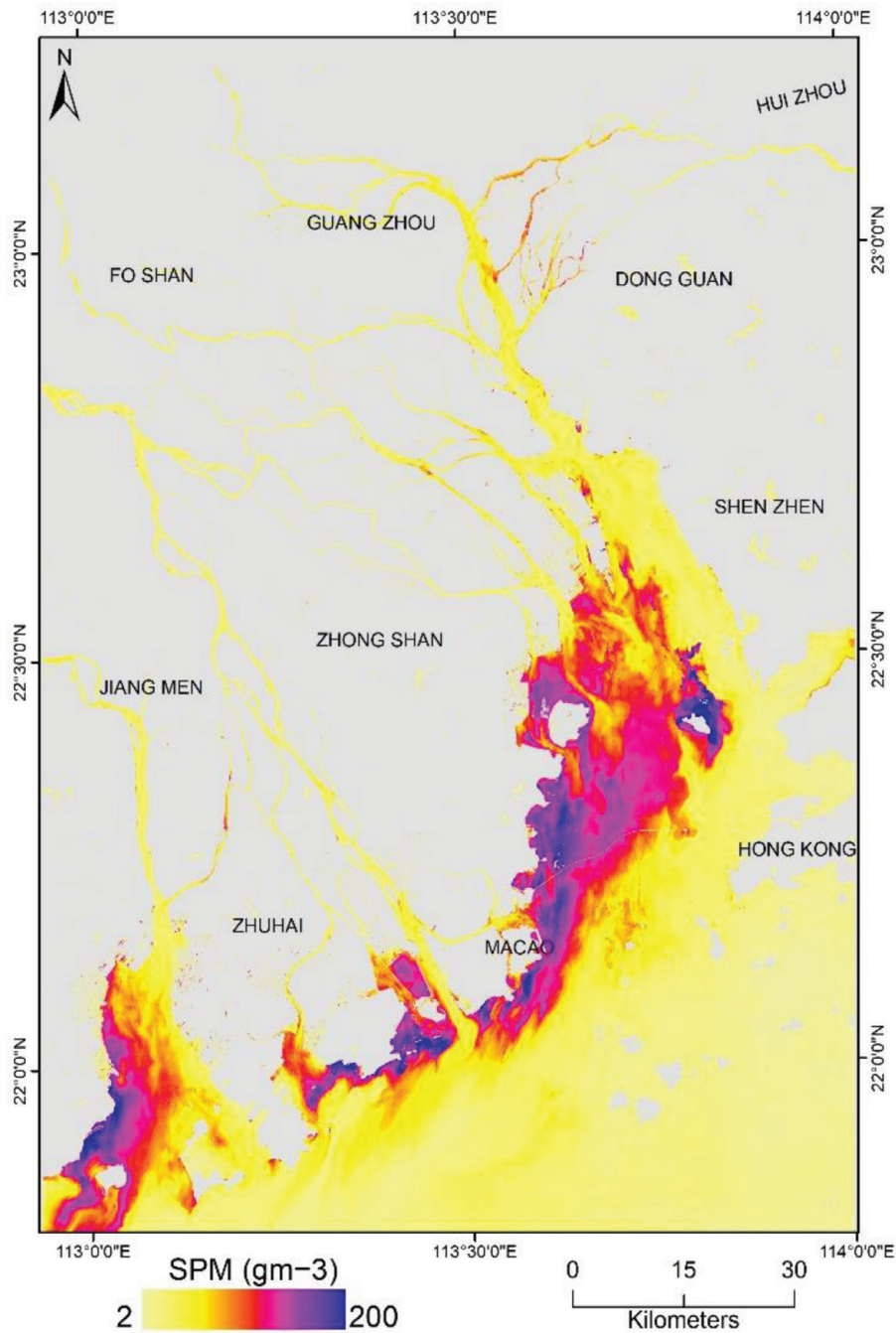


**Figure 9.** High levels of suspended matter concentration were observed in the Pearl River Estuary and its connecting rivers on 31 December 2017.

in an RMSE of 2.60 mg/L. Later, Nazeer et al. [52] evaluated the potential of a machine learning model for estimating TSS in the complex coastal area of Hong Kong achieving an RMSE of 4.59 mg/L. Our work of machine learning models with Landsat TM, ETM+, and OLI data in the same area also shows promising results for estimation of TSS (**Figure 11**). In our work, ANN outperformed the other two machine learning approaches, SVR (support vector machine) and RF (random forest), resulting in the lowest RMSE of 2.8 mg/L. **Table 4** includes some studies and methods used to study TSS in rivers, bays, estuaries, and relatively open coastal waters.

Stormwater runoff is also a large source of marine pollution as runoffs and pollutants from the urban watershed enter into the coastal environment after rainstorms. Stormwater runoff and municipal wastewater plumes may sometimes be overlooked due to persistent cloud cover in optical imagery. These types of

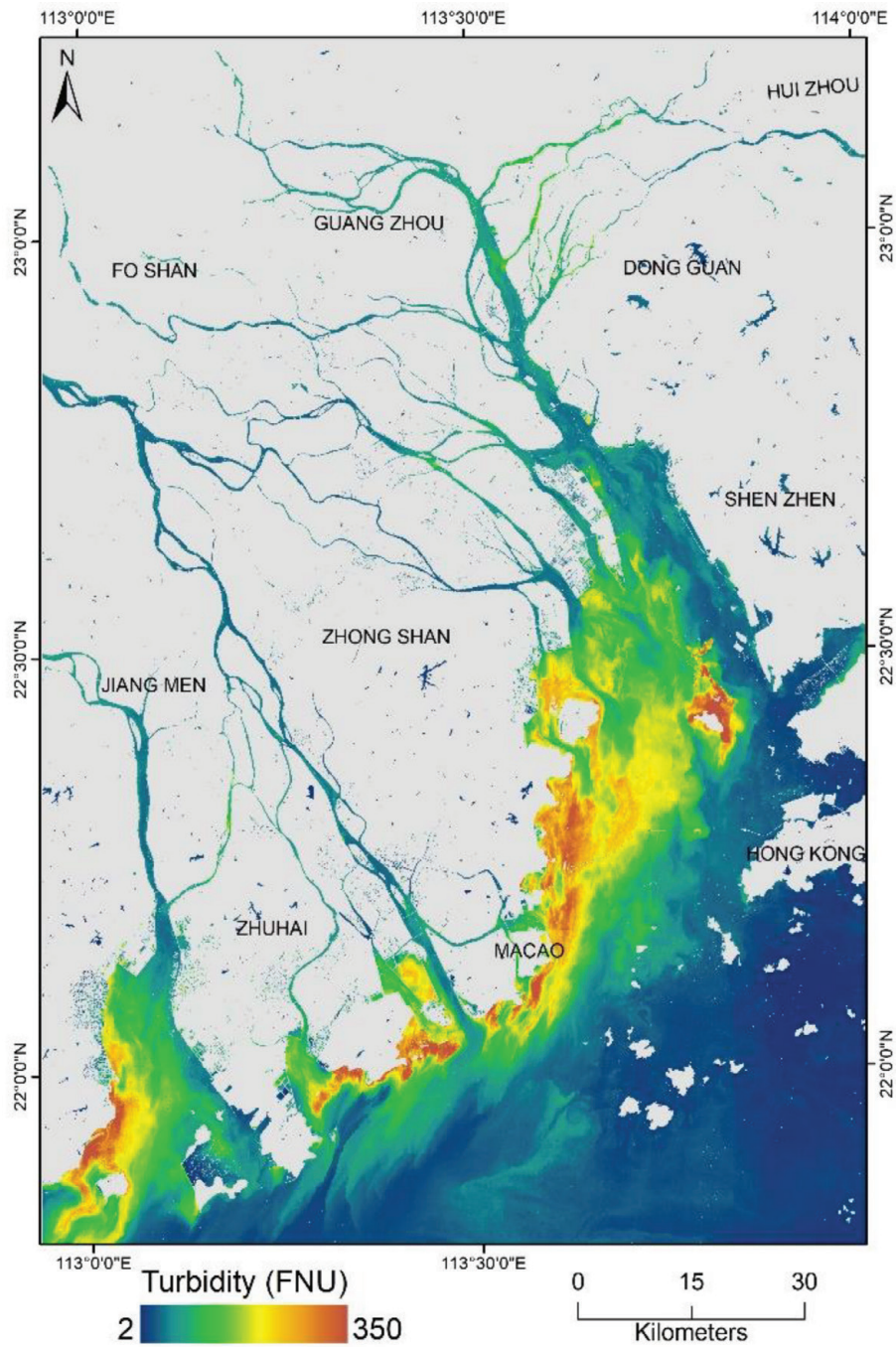


**Figure 10.** High levels of turbidity were observed in the Pearl River Estuary and its connecting rivers on 31 December 2017.

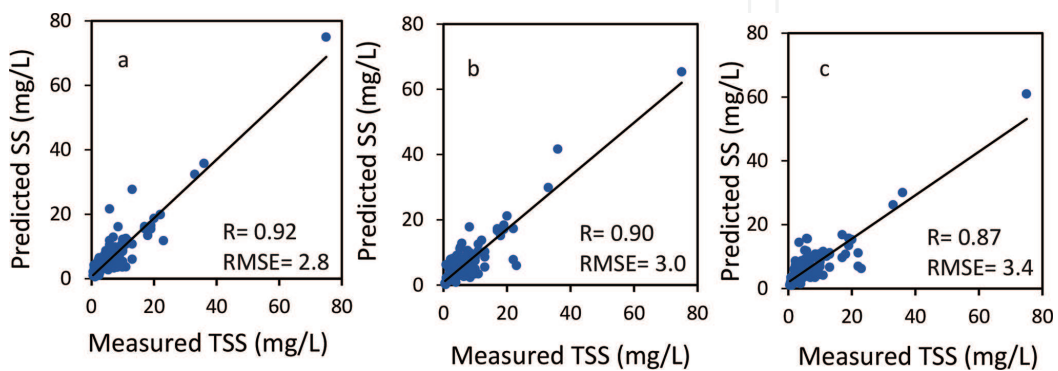


**Figure 11.** Comparison of measured and predicted values from three machine learning models. (a) TSS concentration using artificial neural network, (b) TSS concentration using support vector regression, and (c) TSS concentration using random forest.

| Band combination  |                    | Sensor                              | Reference    |
|---|--------------------|-------------------------------------|--------------|
| All bands (neural network and other machine learning methods) |                    | GOCI                                | [28]         |
|   |                    | Landsat TM, ETM+, OLI, HJ-1 A/B CCD | [52]         |
|   |                    | TM, SAR                             | [45]         |
| Multiple bands and their ratios (multiple regression)         |                    | Landsat OLI band (2–5)              | [19]         |
|   |                    | Landsat ETM+                        | [9]          |
| Multiple green (500–600 nm) and red (600–700 nm) ratio        |                    | Landsat TM, ETM+                    | [68]         |
| Green (500–600 nm) and red (600–700 nm) ratio                 |                    | HJ-1A/1B CCD                        | [67]         |
| Red (600–700 nm) and NIR (700–900 nm) ratio                   |                    | MODIS                               | [65]         |
| Single band algorithms  | Green (500–600 nm) | SeaWiFS                             | [58]         |
|   |                    | EO-ALI                              | [12]         |
|   | Red (600–700 nm)   | Landsat TM, ETM+, HJ-1              | [47, 68]     |
|   |                    | AVHRR, SeaWiFS                      | [58]         |
|   |                    | MODIS, MERIS, SeaWiFS               | [24, 62, 65] |
|   |                    | HICO                                | [17]         |
|   | NIR (700–900 nm)   | MODIS, MERIS, SeaWiFS               | [62]         |

**Table 4.** Methods used to retrieve TSS using remote sensing data in marine waters.

runoff are often detectable via SAR as they deposit surfactants on the sea surface, smoothing the small gravity waves and thus producing an area of low backscatter in comparison to the surrounding sea surface [74]. DiGiacomo et al. [74] used high-resolution SAR to monitor such plumes in the Southern California Bight. In their study, the dynamics of runoff plume was modeled using SAR images together with meteorological data as a function of cumulative event discharge, timing of the peak flow, and total storm precipitation. Holt et al. [75] used multi-platform SAR data along with MODIS and precipitation data to study a stormwater plume and its flow direction.

### 3.3 Oil spill

A large oil spill from tankers causes not only significant economic loss but also destruction to the aquatic ecosystem. After the spill, oil undergoes several processes such as spreading, evaporation, dissolution, drifting, photolysis, biodegradation, and the formation of oil-in-water and water-in-oil emulsions [76].

Owing to the dynamic spreading nature of the spill, both remote and station-based sensors are essential for comprehensive and effective monitoring. Airborne survey of an oil spill can be carried out by side-looking airborne radar (SLAR), laser fluorosensor (LF), and ultraviolet and thermal infrared video cameras. Ultraviolet, microwave, thermal, and optical airborne sensors all exhibit the ability to detect oil spills [6]. Ultraviolet sensors are sensitive to oil thickness of 0.01–0.05  $\mu\text{m}$ . Oil

appears as a bright target in this region of the spectrum, and brightness increases with the thickness of the oil. Optical sensors can measure thicker oil (2–500  $\mu\text{m}$ ) and are able to detect oil dispersed in water, whereas thermal infrared sensors measure oil with a thickness of about 10–50  $\mu\text{m}$  [34]. Airborne LF and microwave radiometers (MWR) are considered to be the most appropriate sensors for oil spill detection. SLAR, ultraviolet, and thermal video cameras were used to identify areas of thick oil during the Sea Empress oil spill in 1996. Oil also undergoes weathering and aging. Multispectral satellite images, taking advantage of fluorescence characteristics of oil, can detect spills and assess the levels of weathering of the oil [31].

Spaceborne synthetic aperture radar (SAR) is commonly used for ocean pollution monitoring, especially oil spills. **Table 5** includes some SAR-equipped satellites used for oil spill detection. The advantage of SAR is the capability to take measurements during all day and all-weather conditions. Therefore, they are considered superior to optical sensors in this application [5]. The spreading trend of oil highly depends on wind direction and speed. An oil spill would break up and disperse if the wind speed is greater than 10 m/s [74]. DiGiacomo et al. [74] used ERS-2 SAR and RADARSAT-1 SAR images to map oil spills in the Southern California Bight. Shirvany et al. [77] evaluated the potential of different polarizations using RADARSAT-2 data for oil spill detection in the Gulf of Mexico. In another study, ENVISAT data was used effectively as an input to a hydrodynamic model to track the fate of oil after the Kerch Strait oil spill in 2007 [78]. **Figure 12** shows an incident of large oil spill on the Galicia coast [79] and the Korean coast [80] for which spaceborne SAR data was used to assess the coverage areas and the damage caused by the spills.

### 3.4 Marine plastic and coastal litter

With the increasing amount of marine plastic litter, its adverse chemical, biological, and ecological impacts on the marine ecosystem have raised the public concerns [81]. It is estimated that 4.8–12.7 million metric tons of plastic is dumped in the sea every year [82] due to increased use of plastic in industry and daily life [83, 84]. Although some surveys have been undertaken [85] to estimate the density and weight of floating plastic in the oceans globally, there is a lack of long-term and large-scale monitoring.

Some research has been conducted using remote sensing technology for the detection of floating marine plastic [86]. However, this research domain is still in its early stages. The reflectance from water captured by sensors is different from that of floating plastic objects. There are several reasons for this, (1) the physical properties of water are different from that of plastic, and they have significant distinct reflectance; (2) the transmitting ability of light through water is different

| Satellite sensor                                 | Operation           |
|--|---------------------|
| Sentinel-1A                                      | 2014, operating     |
| Sentinel-1B                                      | 2016, operating     |
| TerraSAR-X                                       | 2007, operating     |
| ENVISAT advanced synthetic aperture radar (ASAR) | 2002, not operating |
| RADARSAT-1                                       | 1995, not operating |
| European remote sensing (ERS) satellites: ESR-2  | 1995, not operating |

**Table 5.**  
*Active spaceborne sensors mostly used in oil spill detection.*

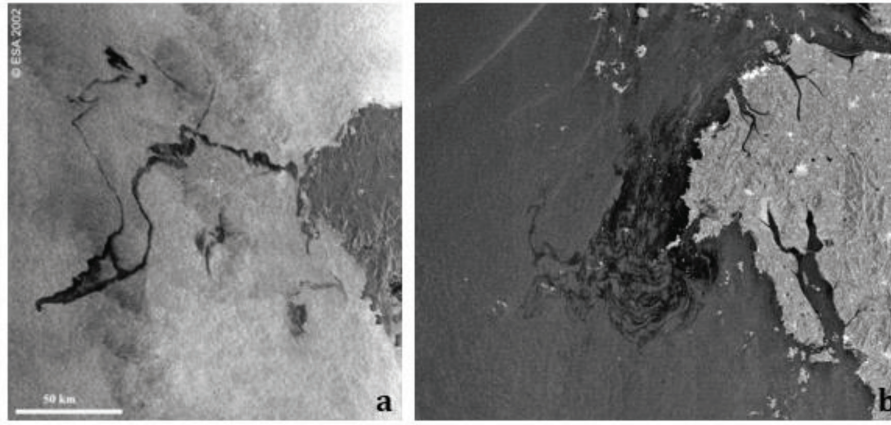


**Figure 12.**

(a) ASAR wide-swath image of northwest coast of Spain, captured on 17 Nov 2002, at 10:45 UTC showing oil from the wrecked tanker approaching Spanish coast (source, ESA), (b) ASAR image of South Korea, captured on 11 Dec 2007, at 01:40 UTC, showing oil spill from 146,000 ton damaged crude oil tanker (source ESA).

from that through plastic; (3) the absorption of light by water is different from plastic [87]. **Figure 13** shows different pathways of incident light after interacting with the surface (with and without marine plastic). Some studies have used hyperspectral remote sensing to study marine macroplastics [87] and microplastics [88]. Goddijn-Murphy et al. [87] considered the spectral signatures and geometric optics of plastic and seawater to develop a reflectance model for detecting macroplastics. The key is to determine the appropriate reflectance peak of plastic and consider its ratio with wavelength bands where water-leaving radiance is low. Their model considers reflectivity of only one type of plastic litter in two dimensions. However, there are some constraints for detecting marine plastics in a real scenario since there have no standard shape, dimension, color, chemical composition, etc. Nevertheless, this study demonstrated the possibility of using remote sensing as a useful means for mapping and tracking of marine plastic.

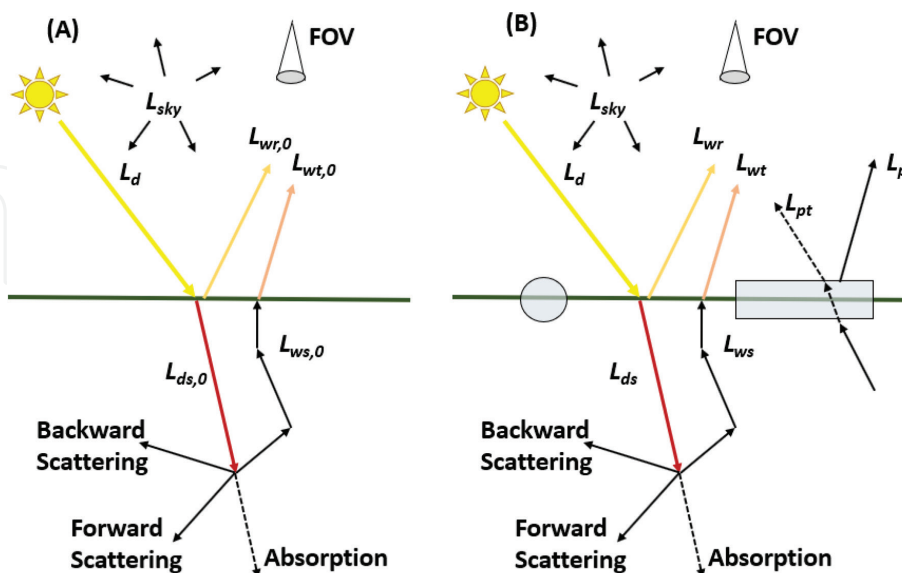


**Figure 13.**

Schematic of solar radiance interacting with (A) an open water body and (B) the same water body but with floating plastic.  $L_d$  is total downwelling radiance (solar beam + diffuse skylight),  $L_{ds}$  is subsurface downwelling radiance,  $L_{ws}$  is subsurface upwelling radiance,  $L_{wr}$  is radiance reflected directly off the water surface,  $L_{wt}$  is subsurface upwelling radiance transmitted through the water-air interface,  $L_{pr}$  is radiance reflected off the plastic, and  $L_{pt}$  is subsurface upwelling radiance transmitted through the plastic.  $L_w$  is total water-leaving radiance,  $L_{wr} + L_{ws}$ , and  $L_p$  is total plastic leaving radiance,  $L_{pt} + L_{pr}$ ; subscript 'o' indicates all the variables in the absence of plastic and FOV is a field of view [87].

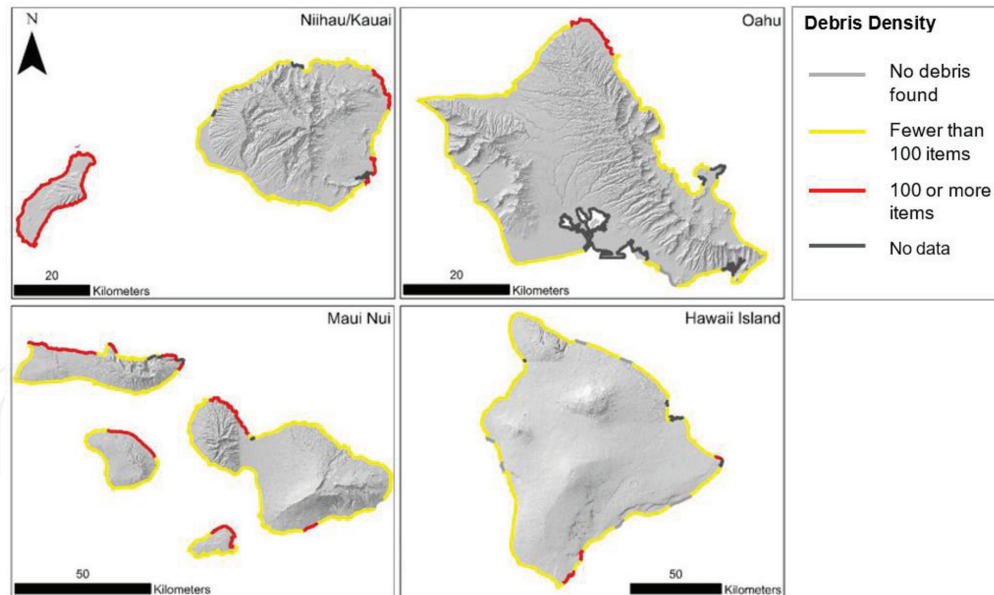


**Figure 14.** Distribution and density of marine litter along the coasts of the main Hawaiian Islands. Areas with 100 and more item densities are shown as hotspots of high marine litter [89].

Detecting coastal litter near land surface is easier than in open ocean, as its reflectance and shape characteristics are not affected by its pitching and rolling on ocean waves. Moy et al. [89] used aerial imagery along with spatial analysis to categorize and map marine litter deposited along the coasts of the Hawaiian Islands. Very high-resolution aerial imagery allowed precise measurements of the quantity, location, type, and size of dumped litter ( $>0.05 \text{ m}^2$ ) (Figure 14). In another study, Martin et al. [90] discussed the potential of combining images from unmanned aerial vehicles (UAV) and a machine learning approach, to detect and map marine litter. Machine learning algorithms are able to detect and classify objects when training samples with known training objects are provided. Their results showed that a UAV-based beach survey is 39 times faster than beach screening on foot and the large footprint of a UAV can cover entire coastlines and beaches including those in remote areas.

#### 4. Conclusion

Increased levels of marine pollution due to anthropogenic activities are adversely affecting marine sustainability of marine ecosystems. Reviewed literature suggested that aerial and spaceborne sensors provide holistic information for monitoring many of the major marine pollutants. These include oil and chemical spills, sewage, high suspended solids, and algal blooms. Solid waste deposited in coastal areas can also be mapped using similar geospatial technology. However, there are some technical limitations in assessing detailed information about pollutants. These limitations stem from their dynamic nature, limited information of specific spectral response of pollutants, substrate response in optically shallow waters, and complex physics of light interaction through the water column. Despite these limitations, remote sensing is still capable of providing useful information about pollution events in sensitive marine areas.

Active and hyperspectral airborne sensors are often considered superior to spaceborne sensors for monitoring coastal and estuarine pollutants due to their real-time and detailed monitoring capability. Spaceborne sensors are more reliable for large-scale ocean, but with the recent development of sensor technology,

especially hyperspectral and active sensors with high temporal resolution, the applications of spaceborne sensors in coastal regions are also increasing. Presently, monitoring of marine waters is offered through numerous satellite sensors such as MODIS, VIIRS, AVHRR, OLCI, GOCI, Landsat, and Sentinel-2 with spectral and spatial resolutions able to measure marine pollutants and other marine parameters. Active satellite sensors such as SAR, altimeters, scanning radiometers, and microwave sounders, which are mostly used in physical oceanography, also possess the potential for detection of marine pollution under specific meteorological conditions and provide useful data to track and model the impact of these pollutants.

Heavy metal pollution in coastal and estuarine region is another major concern of marine managers and researchers. Studies have attempted to use airborne hyperspectral data for this task, but satellite remote sensing is not yet able to detect these loads directly. However, the core factors causing these pollutants such as river plumes, sewerage, and industrial waste entering into these sensitive systems can be monitored using satellite remote sensing. If the point source of heavy metals is traced by remote sensing, policies and management practices can be applied according to the specific pollutants, and their mobilization and transfer of heavy metal to sensitive coastal environments can be avoided. Multiple approaches have proven reliable for this task.

In addition, recent developments in software and computation power have led to the increased use of data captured by remote sensing systems. Computer systems can now store and analyze large datasets. Therefore, marine protection agencies and government can utilize the full potential of remote sensing data in geographic information systems (GIS) and decision support systems (DSS) to manage marine resources and pollution. Collaboration between the research community and government is of utmost importance for using the full potential of this data in marine pollution management. Different applications of remote sensing such as detection of floating marine plastic litter and the use of active remote sensing for detecting algal blooms are still in the research. With the advancement of remote sensing sensors, sophisticated methods will be developed in the future for monitoring marine pollution.

## **Acknowledgements**

Authors would like to acknowledge the General Research Fund (project id: 15246916), the Hong Kong Ph.D. Fellowship Scheme from the Research Grants Council of Hong Kong. The authors would also like to acknowledge US Geological Survey for providing Landsat (TM, ETM+, and OLI) image archive, the Copernicus Open Access Hub for providing Sentinel-2 data, and the Hong Kong Environmental Protection Department for providing station-based coastal water quality data for developing numerical models.

IntechOpen

## Author details

Sidrah Hafeez<sup>1</sup>, Man Sing Wong<sup>1\*</sup>, Sawaid Abbas<sup>1</sup>, Coco Y.T. Kwok<sup>1</sup>, Janet Nichol<sup>1</sup>, Kwon Ho Lee<sup>2</sup>, Danling Tang<sup>3</sup> and Lilian Pun<sup>1</sup>

<sup>1</sup> Department of Land Surveying and Geo-Informatics, The Hong Kong Polytechnic University, Kowloon, Hong Kong

<sup>2</sup> Department of Atmospheric and Environmental Sciences, Gangneung-Wonju National University Gangneung, South Korea

<sup>3</sup> South China Institute of Oceanology Chinese Academy of Sciences, China

\*Address all correspondence to: [lswong@polyu.edu.hk](mailto:lswong@polyu.edu.hk)

## IntechOpen

© 2018 The Author(s). Licensee IntechOpen. This chapter is distributed under the terms of the Creative Commons Attribution License (<http://creativecommons.org/licenses/by/3.0>), which permits unrestricted use, distribution, and reproduction in any medium, provided the original work is properly cited. 

## References

- [1] Clark RB, Frid C, Attrill M. Marine Pollution. Vol. 4. Oxford: Clarendon Press; 1989
- [2] Islam MS, Tanaka M. Impacts of pollution on coastal and marine ecosystems including coastal and marine fisheries and approach for management: A review and synthesis. *Marine Pollution Bulletin*. 2004;**48**:624-649
- [3] Zielinski O, Busch JA, Cembella AD, Daly KL, Engelbrektsson J, Hannides AK, et al. Detecting marine hazardous substances and organisms: Sensors for pollutants, toxins, and pathogens. *Ocean Science*. 2009;**5**:329-349
- [4] ESA. Sentinel-1 Supports Detection of Illegal Oil Spills. 2017. Available from: <https://sentinel.esa.int/web/sentinel/missions/sentinel-1/news/-/article/sentinel-1-supports-detection-of-illegal-oil-spills>
- [5] Brekke C, Solberg AH. Oil spill detection by satellite remote sensing. *Remote Sensing of Environment*. 2005;**95**:1-13
- [6] Zielinski O, Hengstermann T, Robbe N. Detection of oil spills by airborne sensors. In: *Marine Surface Films*. Berlin, Heidelberg: Springer; 2006. pp. 255-271
- [7] Dekker AG, Brando VE, Anstee JM, Pinnel N, Kutser T, Hoogenboom EJ, et al. Imaging spectrometry of water. In: *Imaging Spectrometry*. Dordrecht: Springer; 2002. pp. 307-359
- [8] Pattiaratchi C, Lavery P, Wyllie A, Hick P. Estimates of water quality in coastal waters using multi-date Landsat Thematic Mapper data. *International Journal of Remote Sensing*. 1994;**15**:1571-1584
- [9] Kabbara N, Benkhelil J, Awad M, Barale V. Monitoring water quality in the coastal area of Tripoli (Lebanon) using high-resolution satellite data. *ISPRS Journal of Photogrammetry and Remote Sensing*. 2008;**63**:488-495
- [10] Nas B, Karabork H, Ekercin S, Berktaş A. Mapping chlorophyll-a through in-situ measurements and Terra ASTER satellite data. *Environmental Monitoring and Assessment*. 2009;**157**:375-382
- [11] Chen S, Fang L, Zhang L, Huang W. Remote sensing of turbidity in seawater intrusion reaches of Pearl River Estuary—A case study in Modaomen water way, China. *Estuarine, Coastal and Shelf Science*. 2009;**82**:119-127
- [12] Fang L, Chen S, Wang H, Qian J, Zhang L. Detecting marine intrusion into rivers using EO-1 ALI satellite imagery: Modaomen Waterway, Pearl River Estuary, China. *International Journal of Remote Sensing*. 2010;**31**:4125-4146
- [13] Brando VE, Dekker AG. Satellite hyperspectral remote sensing for estimating estuarine and coastal water quality. *IEEE Transactions on Geoscience and Remote Sensing*. 2003;**41**:1378-1387
- [14] Zhu W, Yu Q. Inversion of chromophoric dissolved organic matter from EO-1 hyperion imagery for turbid estuarine and coastal waters. *IEEE Transactions on Geoscience and Remote Sensing*. 2013;**51**:3286-3298
- [15] Ruiz-Verdú A, Domínguez-Gómez J-A, Peña-Martínez R. Use of CHRIS for monitoring water quality in Rosarito reservoir. In: *Proceedings of the Third Chris Proba Workshop*. ESA-ESRIN; 2005
- [16] Casal G, Kutser T, Domínguez-Gómez J, Sánchez-Carnero N, Freire J. Mapping benthic macroalgal communities in the coastal zone

- using CHRIS-PROBA mode 2 images. *Estuarine, Coastal and Shelf Science*. 2011;**94**:281-290
- [17] Keith DJ, Schaeffer BA, Lunetta RS, Gould RW Jr, Rocha K, Cobb DJ. Remote sensing of selected water-quality indicators with the hyperspectral imager for the coastal ocean (HICO) sensor. *International Journal of Remote Sensing*. 2014;**35**:2927-2962
- [18] Braga F, Giardino C, Bassani C, Matta E, Candiani G, Strömbeck N, et al. Assessing water quality in the northern Adriatic Sea from HICO™ data. *Remote Sensing Letters*. 2013;**4**:1028-1037
- [19] Lim J, Choi M. Assessment of water quality based on Landsat 8 operational land imager associated with human activities in Korea. *Environmental Monitoring and Assessment*. 2015;**187**:384
- [20] Toming K, Kutser T, Laas A, Sepp M, Paavel B, Nõges T. First experiences in mapping lake water quality parameters with Sentinel-2 MSI imagery. *Remote Sensing*. 2016;**8**:640
- [21] Liu H, Li Q, Shi T, Hu S, Wu G, Zhou Q. Application of sentinel 2 MSI images to retrieve suspended particulate matter concentrations in Poyang Lake. *Remote Sensing*. 2017;**9**:761
- [22] O'Reilly JE, Maritorena S, O'Brien MC, Siegel DA, Toole D, Menzies D, Chavez FP. In: *SeaWiFS postlaunch calibration and validation analyses. part 3*. NASA tech. memo. 2000;**206892**(11):3-8
- [23] Miller RL, McKee BA. Using MODIS Terra 250 m imagery to map concentrations of total suspended matter in coastal waters. *Remote Sensing of Environment*. 2004;**93**:259-266
- [24] Chen Z, Hu C, Muller-Karger F. Monitoring turbidity in Tampa Bay using MODIS/Aqua 250 m imagery. *Remote Sensing of Environment*. 2007;**109**:207-220
- [25] Chang N-B, Xuan Z, Yang YJ. Exploring spatiotemporal patterns of phosphorus concentrations in a coastal bay with MODIS images and machine learning models. *Remote Sensing of Environment*. 2013;**134**:100-110
- [26] Shen F, Verhoef W, Zhou Y, Salama MS, Liu X. Satellite estimates of wide-range suspended sediment concentrations in Changjiang (Yangtze) estuary using MERIS data. *Estuaries and Coasts*. 2010;**33**:1420-1429
- [27] Harvey ET, Kratzer S, Philipson P. Satellite-based water quality monitoring for improved spatial and temporal retrieval of chlorophyll-a in coastal waters. *Remote Sensing of Environment*. 2015;**158**:417-430
- [28] Kim YH, Im J, Ha HK, Choi J-K, Ha S. Machine learning approaches to coastal water quality monitoring using GOCI satellite data. *GIScience & Remote Sensing*. 2014;**51**:158-174
- [29] Wang M, Son S. VIIRS-derived chlorophyll-a using the ocean color index method. *Remote Sensing of Environment*. 2016;**182**:141-149
- [30] Toming K, Kutser T, Uiboupin R, Arikas A, Vahter K, Paavel B. Mapping water quality parameters with sentinel-3 ocean and land colour instrument imagery in the Baltic Sea. *Remote Sensing*. 2017;**9**:1070
- [31] Loughland RA, Saji B. Remote sensing: A tool for managing marine pollution in the Gulf. In: *Protecting the Gulf's Marine Ecosystems from Pollution*. Birkhäuser Basel: Springer; 2008. pp. 131-145
- [32] Sherry PL. Applied Remote Sensing Training [Internet]. Available from: <https://arset.gsfc.nasa.gov/sites/default/files/users/fundamentals/fundamentals-aquatic-web.pdf>

- [33] Kaye TG, Falk AR, Pittman M, Sereno PC, Martin LD, Burnham DA, et al. Laser-stimulated fluorescence in paleontology. *PLoS One*. 2015;**10**:e0125923
- [34] Theo Hengstermann NR. Airborne Oil Spill Remote Sensing. *Hydro International*. 2008. Available from: <https://www.hydro-international.com/content/article/airborne-oil-spill-remote-sensing>
- [35] Lee Z, Carder KL, Chen RF, Peacock TG. Properties of the water column and bottom derived from Airborne Visible Infrared Imaging Spectrometer (AVIRIS) data. *Journal of Geophysical Research, Oceans*. 2001;**106**:11639-11651
- [36] Lunetta RS, Knight JF, Paerl HW, Streicher JJ, Peierls BL, Gallo T, et al. Measurement of water colour using AVIRIS imagery to assess the potential for an operational monitoring capability in the Pamlico Sound Estuary, USA. *International Journal of Remote Sensing*. 2009;**30**:3291-3314
- [37] Choe E, van der Meer F, van Ruitenbeek F, van der Werff H, de Smeth B, Kim K-W. Mapping of heavy metal pollution in stream sediments using combined geochemistry, field spectroscopy, and hyperspectral remote sensing: A case study of the Rodalquilar mining area, SE Spain. *Remote Sensing of Environment*. 2008;**112**:3222-3233
- [38] Mouroulis P, Van Gorp B, Green RO, Dierssen H, Wilson DW, Eastwood M, et al. Portable remote imaging spectrometer coastal ocean sensor: Design, characteristics, and first flight results. *Applied Optics*. 2014;**53**:1363-1380
- [39] NASA. NASA Demonstrates Airborne Water Quality Sensor. 2016. Available from: <https://climate.nasa.gov/news/2404/nasa-demonstrates-airborne-water-quality-sensor/>
- [40] A.-A. P. EXperiment. APEX—Airborne Prism EXperiment Flyer. ESA. Winterthurerstrasse, Zurich, Switzerland: University of Zurich; 2012. pp. 5-8
- [41] Gholizadeh MH, Melesse AM, Reddi L. A comprehensive review on water quality parameters estimation using remote sensing techniques. *Sensors*. 2016;**16**:1298
- [42] Moore T. Challenges for Bio-Optical Modeling of Inland Waters. 2017. Available from: <https://iocs.ioccg.org/wp-content/uploads/2017/05/tue-1445-bo4-moore.pdf>
- [43] Gurlin D, Gitelson AA, Moses WJ. Remote estimation of chl-a concentration in turbid productive waters—Return to a simple two-band NIR-red model? *Remote Sensing of Environment*. 2011;**115**:3479-3490
- [44] Gitelson A. The peak near 700 nm on radiance spectra of algae and water: Relationships of its magnitude and position with chlorophyll concentration. *International Journal of Remote Sensing*. 1992;**13**:3367-3373
- [45] Zhang Y, Pulliainen J, Koponen S, Hallikainen M. Application of an empirical neural network to surface water quality estimation in the Gulf of Finland using combined optical data and microwave data. *Remote Sensing of Environment*. 2002;**81**:327-336
- [46] Nazeer M, Nichol JE. Development and application of a remote sensing-based Chlorophyll-a concentration prediction model for complex coastal waters of Hong Kong. *Journal of Hydrology*. 2016;**532**:80-89
- [47] Hellweger F, Schlosser P, Lall U, Weissel J. Use of satellite imagery for water quality studies in New York Harbor. *Estuarine, Coastal and Shelf Science*. 2004;**61**:437-448

- [48] Moses WJ, Bowles JH, Corson MR. Expected improvements in the quantitative remote sensing of optically complex waters with the use of an optically fast hyperspectral spectrometer—A modeling study. *Sensors*. 2015;**15**:6152-6173
- [49] George D. The airborne remote sensing of phytoplankton chlorophyll in the lakes and tarns of the English Lake District. *International Journal of Remote Sensing*. 1997;**18**:1961-1975
- [50] Svejkský J, Shandley J. Detection of offshore plankton blooms with AVHRR and SAR imagery. *International Journal of Remote Sensing*. 2001;**22**:471-485
- [51] Moses WJ, Gitelson AA, Berdnikov S, Saprygin V, Povazhnyi V. Operational MERIS-based NIR-red algorithms for estimating chlorophyll-a concentrations in coastal waters—The Azov Sea case study. *Remote Sensing of Environment*. 2012;**121**:118-124
- [52] Nazeer M, Bilal M, Alsahli MM, Shahzad MI, Waqas A. Evaluation of empirical and machine learning algorithms for estimation of coastal water quality parameters. *ISPRS International Journal of Geo-Information*. 2017;**6**:360
- [53] Wynne T, Stumpf R, Tomlinson M, Warner R, Tester P, Dyble J, et al. Relating spectral shape to cyanobacterial blooms in the Laurentian Great Lakes. *International Journal of Remote Sensing*. 2008;**29**:3665-3672
- [54] Gower J, King S, Borstad G, Brown L. Detection of intense plankton blooms using the 709 nm band of the MERIS imaging spectrometer. *International Journal of Remote Sensing*. 2005;**26**:2005-2012
- [55] Matthews MW, Bernard S, Robertson L. An algorithm for detecting trophic status (chlorophyll-a), cyanobacterial-dominance, surface scums and floating vegetation in inland and coastal waters. *Remote Sensing of Environment*. 2012;**124**:637-652
- [56] Lunetta RS, Schaeffer BA, Stumpf RP, Keith D, Jacobs SA, Murphy MS. Evaluation of cyanobacteria cell count detection derived from MERIS imagery across the eastern USA. *Remote Sensing of Environment*. 2015;**157**:24-34
- [57] Nazeer M, Wong MS, Nichol JE. A new approach for the estimation of phytoplankton cell counts associated with algal blooms. *Science of the Total Environment*. 2017;**590**:125-138
- [58] Myint S, Walker N. Quantification of surface suspended sediments along a river dominated coast with NOAA AVHRR and SeaWiFS measurements: Louisiana, USA. *International Journal of Remote Sensing*. 2002;**23**:3229-3249
- [59] Wass P, Marks S, Finch J, Leeks GJL, Ingram J. Monitoring and preliminary interpretation of in-river turbidity and remote sensed imagery for suspended sediment transport studies in the Humber catchment. *Science of the Total Environment*. 1997;**194**:263-283
- [60] V. e. NASA. Modis: Mouth of the Yangtze. 2018. Available from: <https://visibleearth.nasa.gov/view.php?id=55219>
- [61] Copernicus E. Copernicus Open Access Hub. 2018. Available from: <https://scihub.copernicus.eu/dhus/#/home>
- [62] Nechad B, Ruddick K, Park Y. Calibration and validation of a generic multisensor algorithm for mapping of total suspended matter in turbid waters. *Remote Sensing of Environment*. 2010;**114**:854-866

- [63] Novo E, Hansom J, Curran P. The effect of viewing geometry and wavelength on the relationship between reflectance and suspended sediment concentration. *International Journal of Remote Sensing*. 1989;**10**:1357-1372
- [64] Curran P, Hansom J, Plummer S, Pedley M. Multispectral remote sensing of nearshore suspended sediments: A pilot study. *International Journal of Remote Sensing*. 1987;**8**:103-112
- [65] Feng L, Hu C, Chen X, Song Q. Influence of the Three Gorges Dam on total suspended matters in the Yangtze Estuary and its adjacent coastal waters: Observations from MODIS. *Remote Sensing of Environment*. 2014;**140**:779-788
- [66] Doxaran D, Froidefond J-M, Lavender S, Castaing P. Spectral signature of highly turbid waters: Application with SPOT data to quantify suspended particulate matter concentrations. *Remote Sensing of Environment*. 2002;**81**:149-161
- [67] Tian L, Wai OW, Chen X, Liu Y, Feng L, Li J, et al. Assessment of total suspended sediment distribution under varying tidal conditions in deep bay: Initial results from HJ-1A/1B satellite CCD images. *Remote Sensing*. 2014;**6**:9911-9929
- [68] Nazeer M, Nichol JE. Combining landsat TM/ETM+ and HJ-1 A/B CCD sensors for monitoring coastal water quality in Hong Kong. *IEEE Geoscience and Remote Sensing Letters*. 2015;**12**:1898-1902
- [69] Baban SM. Detecting water quality parameters in the Norfolk Broads, UK, using Landsat imagery. *International Journal of Remote Sensing*. 1993;**14**:1247-1267
- [70] Khorram S, Cheshire H, Geraci AL, ROSA GL. Water quality mapping of Augusta Bay, Italy from Landsat-TM data. *International Journal of Remote Sensing*. 1991;**12**:803-808
- [71] Gholizadeh M, Melesse A. Study on spatiotemporal variability of water quality parameters in Florida Bay using remote sensing. *Journal of Remote Sensing and GIS*. 2017;**6**:2
- [72] Son S, Kim YH, Kwon J-I, Kim H-C, Park K-S. Characterization of spatial and temporal variation of suspended sediments in the Yellow and East China Seas using satellite ocean color data. *GIScience & Remote Sensing*. 2014;**51**:212-226
- [73] Nechad B, Ruddick K, Neukermans G. Calibration and validation of a generic multisensor algorithm for mapping of turbidity in coastal waters. *Remote Sensing of the Ocean, Sea Ice, and Large Water Regions*. 2009;**2009**:74730H
- [74] DiGiacomo PM, Washburn L, Holt B, Jones BH. Coastal pollution hazards in southern California observed by SAR imagery: Stormwater plumes, wastewater plumes, and natural hydrocarbon seeps. *Marine Pollution Bulletin*. 2004;**49**:1013-1024
- [75] Holt B, Trinh R, Gierach MM. Stormwater runoff plumes in the Southern California Bight: A comparison study with SAR and MODIS imagery. *Marine Pollution Bulletin*. 2017;**118**:141-154
- [76] Daling PS, Brandvik PJ, Mackay D, Johansen O. Characterization of crude oils for environmental purposes. *Oil and Chemical Pollution*. 1990;**7**: 199-224
- [77] Shirvany R, Chabert M, Tourneret J-Y. Ship and oil-spill detection using the degree of polarization in linear and hybrid/compact dual-pol SAR. *IEEE Journal of Selected Topics in Applied Earth Observations and Remote Sensing*. 2012;**5**:885-892

- [78] Korshenko A. Oil Spill Accident in the Kerch Strait in November 2007. Moscow, Russia: Nauka; 2011
- [79] Carracedo P, Torres-López S, Barreiro M, Montero P, Balseiro C, Penabad E, et al. Improvement of pollutant drift forecast system applied to the Prestige oil spills in Galicia Coast (NW of Spain): Development of an operational system. *Marine Pollution Bulletin*. 2006;**53**:350-360
- [80] Kim D-J, Moon WM, Kim Y-S. Application of TerraSAR-X data for emergent oil-spill monitoring. *IEEE Transactions on Geoscience and Remote Sensing*. 2010;**48**:852-863
- [81] Rochman CM, Browne MA, Underwood A, Franeker JA, Thompson RC, Amaral-Zettler LA. The ecological impacts of marine debris: Unraveling the demonstrated evidence from what is perceived. *Ecology*. 2016;**97**:302-312
- [82] Jambeck JR, Geyer R, Wilcox C, Siegler TR, Perryman M, Andrady A, et al. Plastic waste inputs from land into the ocean. *Science*. 2015;**347**:768-771
- [83] Andrady AL, Neal MA. Applications and societal benefits of plastics. *Philosophical Transactions of the Royal Society, B: Biological Sciences*. 2009;**364**:1977-1984
- [84] Andrady AL. Persistence of plastic litter in the oceans. In: *Marine Anthropogenic Litter*. Cham: Springer; 2015. pp. 57-72
- [85] Eriksen M, Lebreton LC, Carson HS, Thiel M, Moore CJ, Borerro JC, et al. Plastic pollution in the world's oceans: More than 5 trillion plastic pieces weighing over 250,000 tons afloat at sea. *PLoS One*. 2014;**9**:e111913
- [86] Maximenko N, Arvesen J, Asner G, Carlton J, Castrence M, Centurioni L, et al. Remote sensing of marine debris to study dynamics, balances and trends. In: *Community White Paper Produced at the Workshop on Mission Concepts for Marine Debris Sensing*. 2016
- [87] Goddijn-Murphy L, Peters S, van Sebille E, James NA, Gibb S. Concept for a hyperspectral remote sensing algorithm for floating marine macroplastics. *Marine Pollution Bulletin*. 2018;**126**:255-262
- [88] Serranti S, Palmieri R, Bonifazi G, Cózar A. Characterization of microplastic litter from oceans by an innovative approach based on hyperspectral imaging. *Waste Management*. 2018;**76**:117-125
- [89] Moy K, Neilson B, Chung A, Meadows A, Castrence M, Ambagis S, et al. Mapping coastal marine debris using aerial imagery and spatial analysis. *Marine Pollution Bulletin*. 2018;**132**:52-59
- [90] Martin C, Parkes S, Zhang Q, Zhang X, McCabe MF, Duarte CM. Use of unmanned aerial vehicles for efficient beach litter monitoring. *Marine Pollution Bulletin*. 2018;**131**:662-673